Bioorganic Chemistry 151 (2024) 107706

Contents lists available at ScienceDirect

Bioorganic Chemistry

journal homepage: www.elsevier.com/locate/bioorg

New cyclometalated iridium(III) complexes bearing substituted 2-(1H-benzimidazol-2-yl)quinoline: Synthesis, characterization, electrochemical and anticancer studies

Cigdem Sahin [a,*], Dogukan Mutlu [b,**], Ahmet Erdem [c], Rafet Kilincarslan [d,***], Sevki Arslan [b]

[a] Department of Engineering Basic Sciences, Faculty of Engineering and Natural Sciences, Istanbul Medeniyet University, Istanbul, Turkey
[b] Department of Biology, Faculty of Science, Pamukkale University, Denizli, Turkey
[c] Advanced Technology Application and Research Center, Pamukkale University, Denizli, Turkey
[d] Department of Chemistry, Faculty of Science, Pamukkale University, Denizli, Turkey

ARTICLE INFO

Keywords:
Iridium complex
2-(1H-benzimidazol-2-yl)quinoline
Cytotoxicity
Apoptosis

ABSTRACT

New iridium(III) compounds ($\mathbf{C_1}$–$\mathbf{C_3}$) bearing 2-(1H-benzimidazol-2-yl)quinoline ligands with different side groups (benzyl, 2,3,4,5,6-pentamethylbenzyl and 2,3,4,5,6-pentafluorobenzyl) were synthesized and characterized by using spectroscopic analyses. The effects of different side groups of iridium compounds on the photophysical and electrochemical properties have been investigated. The cytotoxicity and apoptosis of the compounds have been evaluated on breast cancer cell lines using various methods including MTT assay, flow cytometry, qRT-PCR, and colony formation. The cytotoxicity of $\mathbf{C_1}$, expressed as IC50 values, was found to be 11.76 μM for MDA-MB-231 and 5.35 μM for MCF-7 cells. For $\mathbf{C_3}$, the IC50 value was 16.22 μM for MDA-MB-231 and 8.85 μM for MCF-7 cells. In both cell lines, increased levels of Bax and caspase 3, along with downregulation of BCL-2 and positive annexin V staining, were observed, confirming apoptosis. Moreover, the colony-forming abilities in both cell lines decreased after $\mathbf{C_1}$ and $\mathbf{C_3}$ complex treatment. All these results suggest that the compounds $\mathbf{C_1}$ and $\mathbf{C_3}$ may have potential in the treatment of breast cancer, though further research is needed to confirm their efficacy.

1. Introduction

Cancer is an important health problem that is growing rapidly on a global scale [1,2]. Cancer includes hundreds of distinct types, each affecting various organs, tissues, and cells (colon, liver, lung, breast, etc.). These malignancies manifest as carcinomas, lymphomas, sarcomas, or leukemias, each requiring specific therapeutic strategies [3]. The predominant clinical approaches for cancer treatment comprise chemotherapy, hormone therapy, radiation therapy, surgical intervention, and targeted therapy utilizing anticancer agents [4]. The need for novel and better pharmacological therapies for cancer treatment still exists. The development of efficacious antineoplastic agents with low toxicity and high specificity presents a significant challenge for the scientific community [4–6]. The efficiency of cisplatin and its related compounds in overcoming cancer has triggered intensive research efforts in the investigation of new anti-cancer metallo drugs [7]. Platin-based drugs are used in the treatment of a range of cancers, such as bladder, ovarian, lung, neck and head cancer [7–9]. However, they have some disadvantages. The major obstacles to the development process have been the intrinsic or acquired resistance and severe side effects associated with platinum-based drugs [10–12]. In light of this understanding, the evaluation of more effective, less toxic, non-resistant metal complexes has attracted more attention [13]. Recently, organoiridium-based compounds have been reported as anticancer agents that overcome cisplatin resistance effectively or accelerate the death of cancer cells by paraptotic, apoptotic, and autophagic ways [14,15]. The use of cyclometalated iridium(III) complexes as biosensing agents and bioimaging is due to their good cell permeability and efficient photophysical properties [16,17] depending on the nature and binding pattern of the ligand. The complexes have been implicated as selective

* Corresponding author.
** Corresponding author.
*** Corresponding author.
E-mail addresses: cigdem.sahin@medeniyet.edu.tr (C. Sahin), dogukanmutlu@gmail.com (D. Mutlu), rkilincarslan@pau.edu.tr (R. Kilincarslan).

https://doi.org/10.1016/j.bioorg.2024.107706
Received 28 June 2024; Received in revised form 30 July 2024; Accepted 6 August 2024
Available online 8 August 2024

organelle agents such as mitochondrion, nucleus, and endoplasmic reticulum [18,19]. The enormous potential to be discovered as organelle-selected anticancer agents increases the importance of cyclometalated iridium(III) complexes, biological activity can be perfected by ligand design [20]. The benzimidazole derivatives as ligands can allow the formation of diverse interactions with DNA which may provide high selectivity and effective anticancer activity towards cancer cells [21,22]. The photophysical, photochemical, and biological activity of iridium complexes are considerably tuned using various substituents on benzimidazole ligands [23].

Herein, we report the synthesis, characterization, and anticancer properties of iridium(III) compounds (**C_1**–**C_3**) bearing substituted 2-(1H-benzimidazol-2-yl)quinoline derivatives. The cytotoxicity and apoptosis of the compounds with different side groups (benzyl, 2,3,4,5,6-pentamethylbenzyl and 2,3,4,5,6-pentafluorobenzyl) on 2-(1H-benzimidazol-2-yl)quinoline have been evaluated on breast cancer cell lines (MDA-MB-231 and MCF-7) by the MTT assay, colony formation assay, flow cytometry, and qRT-PCR methods.

2. Experimental

2.1. Materials and methods

All materials, reagents and solvents were purchased from commercial suppliers (Sigma-Aldrich and Merck) and used without further purification. 2-(1H-benzimidazol-2-yl)quinoline (**QuBim**) [24–26], 2-(1-benzyl-1H-benzimidazol-2-yl)quinoline (**L_1**), 2-[1-(2,3,4,5,6-pentamethyl benzyl)-1H-benzimidazol-2-yl]quinoline (**L_2**) [26,27] and $Ir_2(ppy)_4Cl_2$ (ppy: 2-phenylpyridine) [28] were synthesized as previously described. FTIR-ATR spectra were recorded on Perkin Elmer Spectrum Two FT-IR Spectrometer. NMR spectra were acquired on a Varian Mercury AS 400 NMR instrument at 400 MHz (^{1}H) and 100.56 MHz (^{13}C). The mass spectra were obtained from Thermo scientific TSQ quantis LC-MS/MS system. The photoluminescence (PL) and UV–Vis absorption spectra were performed using Perkin Elmer LS55 fluorescence spectrometer and Shimadzu UV-1601 UV–Vis spectrophotometer, respectively. The PL quantum yields of the compounds were calculated according to literature using $Ru(bipyridine)_3(PF_6)_2$ as reference material (Φ_{PL}=0.095 in acetonitrile) [29]. Electrochemical studies were carried out using Drop Sens μStat 200 bipotentiostat in tetrabutylammonium hexafluorophosphate ($TBAPF_6$) acetonitrile solution (0.1 M). Glassy carbon, silver wire and Pt wire counter were used as working electrode, reference electrode and counter electrode, respectively.

2.2. Synthesis and characterization

2.2.1. Synthesis of 2-[1-(2,3,4,5,6-pentafluorobenzyl)-1H-benzimidazol-2-yl]quinoline (**L_3**)

L_3 ligand was synthesized starting from QuBim as in our previous report [26,27]. QuBim (10.0 mmol) and KOH (10.0 mmol) were stirred in a Schlenk tube at 40 °C for 2 h in toluene. At the end of the time, 2,3,4,5,6-pentafluorobenzyl bromide (11.0 mmol) was added, and the mixture was refluxed for 8 h. The solvent was removed in vacuo, and the residue was filtered by adding CH_2Cl_2. The filtrate was allowed to crystallize by adding hexane. 78 % yield. FTIR (ATR), cm^{-1}): 3466, 3056, 2941, 2857, 1950, 1929, 1887, 1810, 1737, 1641, 1615, 1598, 1565, 1498, 1444,1425, 1390, 1287, 1259, 1208, 1120, 1073, 921, 839, 758, 716, 731. ^{1}H NMR ($CDCl_3$, 400 MHz, δ ppm): 6.67 (s, 2H, N-C*H*$_2$); 7.32–7.36 (m, 2H, Ar-*H*); 7.39–7.43 (m, 1H, Ar-*H*); 7.59 (td, 1H, J = 7.5 Hz, J = 1.2 Hz, J = 0.8 Hz, Ar-*H*); 7.75 (td, 1H, J = 7.7 Hz, J = 1.4 Hz, J = 1.4 Hz, Ar-*H*); 7.86–7.90 (m, 2H, Ar-*H*); 8.08 (d, 1H, J = 8.4 Hz, Ar-*H*); 8.32 (d, 1H, J = 8.4 Hz, Ar-*H*); 8.57 (d, 1H, J = 8.4 Hz, Ar-*H*). ^{13}C NMR ($CDCl_3$, 100.56 MHz, δ ppm): 37,90 (N-*C*H$_2$), 109,65, 120.68, 121.81, 123.25, 124.31, 127.47, 127.83, 127.87, 129.31, 130.00, 136.29, 136.95 (Ar-*C*, QuBim) 138.77, 139.57, 144.04, 146.51 (Ar-*C*, $C_6(F)_5$–2,3,4,5,6) 142.58, 146.93, 149.76, 150.44 (Ar-*C*, QuBim).

2.2.2. Synthesis of cyclometalated iridium(III) complexes (**C_1**–**C_3**)

The cyclometalated iridium(III) complexes (**C_1**–**C_3**) were synthesized according to literature procedure with some modifications [30]. $Ir_2(ppy)_4Cl_2$ dimer (0.5 mmol) and the corresponding 2-(1H-benzimidazol-2-yl)quinoline ligand (**L_1**, **L_2** or **L_3**) (1.1 mmol) in 2-ethoxyethanol (10.0 mL) were refluxed for 24 h under argon atmosphere. After cooling to room temperature, aqueous KPF_6 was added to the reaction mixture. The resulting orange precipitate was filtered and washed with deionized water. Then, the crude product was purified by column chromatography (silica gel: CH_2Cl_2/acetone (5/0.25) and an orange solid was obtained.

$[Ir(ppy)_2L_1][PF_6]$ (**C_1**)*:* 81 % yield. FTIR (ATR, cm^{-1}): 3044, 1607, 1584, 1523, 1478, 1422, 1328, 1164, 834. ^{1}H NMR (DMSO-d_6, 400 MHz) δ ppm: 8.76 (d, J = 8.4 Hz, 1H, Ar-*H*), 8.51 (d, J = 9.2 Hz, 1H, Ar-*H*), 8.25 (d, J = 8.4 Hz, 1H, Ar-*H*), 8.08 (d, J = 8.8 Hz, 2H, Ar-*H*), 8.03 (d, J = 8.4 Hz, 1H, Ar-*H*), 7.96–7.88 (m 4H, Ar-*H*), 7.82–7.75 (m, 3H, Ar-*H*), 7.57 (t, J = 7.2 Hz, 1H, Ar-*H*), 7.40 (t, J = 7.2 Hz, 1H, Ar-*H*), 7.35–7.25 (m, 3H, Ar-*H*), 7.17 (t, J = 7.6 Hz, 1H, Ar-*H*), 7.12–7.08 (m, 4H, Ar-*H*), 7.04–6.93 (m, 4H, Ar-*H*), 6.89 (t, J = 7.6 Hz, 1H, Ar-*H*), 6.33 (q, J = 18.0 Hz, 3H, Ar-*H,* N-C*H*$_2$), 6.13 (d, J = 7.6 Hz, 1H, Ar-*H*), 6.01 (d, J = 7.2 Hz, 1H, Ar-*H*). ^{13}C NMR (DMSO-d_6, 100.57 MHz) δ ppm: 167.5, 166.8, 154.8, 152.9, 151.0, 149.2, 147.9, 144.6, 144.2, 141.6, 139.5, 139.0, 137.4, 136.0, 132.0, 130.7, 130.2, 129.6, 129.4, 129.2, 128.5, 128.3, 126.7, 126.4, 125.7, 125.3, 123.8, 123.0, 122.4, 121.5, 120.3, 120.1, 113.2 (Ar-*C*) 49.2 (N-*C*H$_2$) ESI-MS (m/z) = 836.02 [M-PF_6]$^+$.

$[Ir(ppy)_2L_2][PF_6]$ (**C_2**)*:* 72 % yield. FTIR (ATR, cm^{-1}): 3045, 2985, 1606, 1584, 1510, 1478, 1423, 1323, 1163, 837. ^{1}H NMR (DMSO-d_6, 400 MHz) δ ppm: 8.86 (d, J = 8.4 Hz, 1H, Ar-*H*), 8.67 (d, J = 8.4 Hz, 2H, Ar-*H*), 8.20 (d, J = 8.4 Hz, 1H, Ar-*H*), 8.11 (d, J = 8.4 Hz, 1H, Ar-*H*), 8.06 (d, J = 8.4 Hz, 1H, Ar-*H*), 7.98 (d, J = 9.6 Hz, 1H, Ar-*H*), 7.90–7.71 (m, 6H, Ar-*H*), 7.56 (t, J = 7.6 Hz, 1H, Ar-*H*), 7.52 (d, J = 5.6 Hz, 1H, Ar-*H*), 7.26 (t, J = 7.6 Hz, 1H, Ar-*H*), 7.18 (t, J = 7.2 Hz, 1H, Ar-*H*), 7.08–6.92 (m, 6H, Ar-*H*), 6.85 (q, J = 8.4 Hz, 2H, N-C*H*$_2$), 6.31 (d, J = 7.2 Hz, 1H, Ar-*H*), 6.09 (d, J = 7.6 Hz, 1H, Ar-*H*), 5.83 (d, J = 8.4 Hz, 1H, Ar-*H*), 2.46 (s, 15H, 2,3,4,5,6-(C*H*$_3$)$_5$-C$_6$). ^{13}C NMR (DMSO-d_6, 100.57 MHz) δ ppm: 167.5, 166.8, 154.7, 153.2, 151.9, 151.1, 150.1, 147.9, 145.1, 144.6, 144.3, 139.4, 138.9, 137.4, 130.8, 130.2, 129.5, 129.2, 128.5, 128.3, 123.6, 122.9, 120.4, 120.1 (Ar-*C*), 117.7, 113.5, 53.4 (N-*C*H$_2$), 17.9 2,3,4,5,6-(*C*H$_3$)$_5$-C$_6$. ESI-MS (m/z) = 905.52 [M-PF_6]$^+$.

$[Ir(ppy)_2L_3][PF_6]$ (**C_3**)*:* 78 % yield. FTIR (ATR, cm^{-1}): 3052, 1607, 1587, 1505, 1478, 1425, 1331, 1125, 833. ^{1}H NMR (DMSO-d_6, 400 MHz) δ ppm: 8.88 (d, J = 8.8 Hz, 1H, Ar-*H*), 8.69 (d, J = 8.8 Hz, 1H, Ar-*H*), 8.19 (d, J = 7.6 Hz, 1H, Ar-*H*), 8.08 (t, J = 8.0 Hz, 2H, Ar-*H*), 8.02 (d, J = 8.4 Hz, 1H, Ar-*H*), 7.93 (d, J = 5.2 Hz, 1H, Ar-*H*), 7.89–7.79 (m, 4H, Ar-*H*), 7.75 (d, J = 6.8 Hz, 2H, Ar-*H*), 7.58 (t, J = 6.8 Hz, 1H, Ar-*H*), 7.41 (t, J = 8.0 Hz, 1H, Ar-*H*), 7.17 (t, J = 6.8 Hz, 1H, Ar-*H*), 7.07 (t, J = 7.2 Hz, 1H, Ar-*H*), 7.00–6.94 (m, 4H, Ar-*H*), 6.87 (t, J = 7.6 Hz, 1H, Ar-*H*), 6.47 (q, J = 17.6 Hz, 3H, Ar-*H,* N-C*H*$_2$), 6.27 (d, J = 7.2 Hz, 1H, Ar-*H*), 6.09 (d, J = 6.8 Hz, 1H, Ar-*H*), 5.97 (d, J = 8.8 Hz, 1H, Ar-*H*). ^{13}C NMR (DMSO-d_6, 100.57 MHz) δ ppm: 167.4, 166.6, 155.2, 152.5, 151.03, 149.0, 148.0, 146.6, 144.6, 144,09, 143.8, 141.5, 141.2, 139.3, 138.9, 137.1, 131.96, 130.9, 130.3, 129.7, 129.3, 128.1, 125.7, 125.3, 124.2, 123.5, 123.1, 122.4, 121.7, 120.3, 120.2, 118.0, 112.9 (Ar-*C*), 44.03 (N-*C*H$_2$). ESI-MS (m/z) = 925.33 [M-PF_6]$^+$.

2.3. Cell culture and viability

The human breast cell lines (MDA-MB-231 and MCF-7) and human embryonic kidney (HEK293) cell line were obtained from European Collection of Authenticated Cell Cultures (ECACC). Cells were maintained in DMEM or RPMI 1640 (Sigma-Aldrich, Germany) supplemented with 10 % fetal bovine serum (FBS) (Capricorn, Germany) and 1 % penicillin/streptomycin mix (Capricorn, Germany). The cells were cultured in 100 mm diameter culture dishes at 37 °C in a humidified incubator containing 5 % CO2 and grown until 90 % confluent. Approximately, 2 × 10^3 cells were seeded in 96-well plate (Costar,

Corning, USA) and treated with various concentrations (15.6–250 μM) of compounds dissolved in DMSO (not exceed 1 %) after 24 h as described previously [31]. 50 μM cisplatin was used as a positive control. After that, MTT solution (5 mg/mL) (Merck, Germany) was added to each well and incubated for 4 h. In each well, 50 μL dimethyl sulfoxide (DMSO) (Carlo Erba, Germany) was added to dissolve the formazan dye. The absorbance was measured by a microplate reader (Epoch, BioTek, USA) at 590 nm. Cell viability was calculated as a percentage of the control. The obtained data were used to estimate the 50 % inhibitory concentration (IC_{50}) values and calculations were evaluated by GraphPad Prism® software v.9.

2.4. Colony formation

To assess the effect of compounds on colony formation capabilities, MDA-MB-231 and MCF-7 cells were seeded in 6-well plates with 1×10^3 cells/well and treated for 24 h. Control cells were treated with DMSO only (v/v). After 24 h, mediums were refreshed with culture medium and maintained for at least one week. The cells were fixed with 100 % methanol for 10 min and then stained with 0.1 % crystal violet for 15 min. After staining, the wells were washed with PBS 2–3 times and dried overnight. The colonies were observed by inverted microscope, captured, and analyzed by ImageJ software 1.53e as described previously [32].

2.5. Flow cytometry analysis

The apoptosis was evaluated using the Annexin V-APC/7-AAD Apoptosis Kit Detection (K101, BioVision) according to the manufacturer's instructions as described previously [33]. The MDA-MB-231 and MCF-7 cells were seeded in 6-well plates (3×10^4 cells/well) and treated with $\mathbf{C_1}$ and $\mathbf{C_3}$ at IC_{50} concentration. 0.2 mM hydrogen peroxide (H_2O_2) was used a positive control. After 24 h of incubation, cells were collected with 0.25 % Trypsin-EDTA. Afterwards, cells washed with PBS and resuspended in cold binding buffer. Cells were stained with 10 μL propidium iodide (PI) and 5 μL Annexin V-APC. After, cell suspensions were incubated for 15 min in the darkroom. Lastly, 400 μl of Annexin V binding buffer was added to each tube and the samples were analyzed using flow cytometry (CytoFlex, Beckman Coulter) to determine the percentage of apoptotic cells with CytExpert Software.

2.6. Quantitative real-time RT-PCR

The effect of $\mathbf{C_1}$ and $\mathbf{C_3}$ on the expression of *Bcl-2*, *BAX*, *CASP3*, *CASP8*, and *CASP9* genes in breast cancer cells was investigated by SYBR green quantitative PCR assay. The cancer cells (about 3×10^4 cells) were treated with the compounds at IC_{50} concentration for 24 h, total RNA of the cells was extracted using the innuPREP RNA Mini Kit 2.0 (Analytik Jena, Germany), and OneScript® Plus cDNA Synthesis Kit (ABM, USA) was used for cDNA synthesis according to the manufacturer's instructions. RT-PCR was performed using ABM KiloGreen 2X qPCR MasterMix (USA) in an Applied Biosystems™ StepOnePlus™ Real-Time PCR System (Thermo Fisher Scientific Inc., USA). GAPDH, a reliable housekeeping gene, was used as an internal control. The sequence of the primers used in this study was presented in Table 1. For the determination of mRNA levels, the $2^{-\Delta\Delta Ct}$ method was used as described previously [34].

Table 1
The sequences of primers used in this study.

Genes	Forward primer 5′-3′	Reverse primer 3′-5′
GAPDH	GTCTCCTCTGACTTCAACAGCG	ACCACCCTGTTGCTGTAGCCAA
Bcl-2	ATCGCCCTGTGGATGACTGAGT	GTCTCCTCTGACTTCAACAGCG
BAX	GTCTCCTCTGACTTCAACAGCG	ACCACCCTGTTGCTGTAGCCAA
CASP3	GGAAGCGAATCAATGGACTCTGG	GCATCGACATCTGTACCAGACC
CASP8	AGAAGAGGGTCATCCTGGGAGA	TCAGGACTTCCTTCAAGGCTGC
CASP9	GTTTGAGGACCTTCGACCAGCT	CAACGTACCAGGAGCCACTCTT

2.7. Statistical analysis

GraphPad Prism 9.0 software was used for statistical analyses. The results were presented as the means ± SD of at least three replicates. The statistical differences between the groups were analyzed by One-way ANOVA. P-values < 0.05 were statistically significant.

3. Results and discussion

3.1. Synthesis and characterization

The cyclometalated iridium compounds were synthesized using a bridge-splitting reaction of $Ir_2(ppy)_4Cl_2$ dimer with the corresponding 2-(1H-benzimidazol-2-yl)quinoline ligand ($\mathbf{L_1}$, $\mathbf{L_2}$ or $\mathbf{L_3}$) in 2-ethoxyethanol under reflux conditions (Scheme 1) [30]. The compounds were obtained as their PF_6 salts by ion exchange from Cl^- to PF_6^-. The characterization of the compounds was analyzed by FTIR, mass, ^1H and ^{13}C NMR spectroscopies (Figs. S1–S8). The FTIR spectra of the compounds ($\mathbf{C_1}$–$\mathbf{C_3}$) show the characteristic vibration bands of C═N and C═C of 2-phenylpyridine and 2-(1H-benzimidazol-2-yl)quinoline ligands in the 1607–1422 cm^{-1} range. The strong band at around 836 cm^{-1} is assigned to the PF_6^- counter anion of the compounds [35]. In the ^1H NMR spectra of the compounds ($\mathbf{C_1}$–$\mathbf{C_3}$), the ratios of the aromatic peaks exhibit the presence of 2-(1H-benzimidazol-2-yl)quinoline and 2-phenylpyridine ligands between 5.83 and 8.88 ppm. The signal at around 7.75 ppm was observed due to the proton adjacent to N atom of 2-phenylpyridine [36]. The aromatic proton peaks of 2-(1H-benzimidazol-2-yl)quinoline derivatives in the compounds ($\mathbf{C_1}$–$\mathbf{C_3}$) at around 8.76, 8.67, 7.40 and 6.00 ppm are in good agreement with the reported iridium compounds bearing benzimidazole and 2-phenylpyridine ligands [30,37]. The peak at around 6.47 ppm was observed due to the benzylic CH_2 protons of the benzimidazol fragment in the compounds. The characteristic signal of methyl group of $\mathbf{L_2}$ was appeared as a singlet at 2.46 ppm for the compound $\mathbf{C_2}$. In the ^{13}C NMR spectra of the compounds, the signals of the cyclometalation carbon bound to iridium and the carbon atom adjacent to N atom of 2-phenylpyridine atom were observed at around 147.9 ppm and 151 ppm [36,38,39]. The signals at around 44 ppm are associated with the benzylic CH_2 carbon of the benzimidazol fragment of the compounds ($\mathbf{C_1}$–$\mathbf{C_3}$). The ESI mass spectra of $\mathbf{C_1}$–$\mathbf{C_3}$ exhibited the parent molecular $[M\text{-}PF_6]^+$ which supported the formation of compounds.

3.2. The photophysical and electrochemical studies

The absorption and photoluminescence (PL) spectra of the compounds ($\mathbf{C_1}$–$\mathbf{C_3}$) have been investigated at room temperature in acetonitrile solution (1×10^{-5} M) (Fig. 1 and Table 2). The absorption maxima of $\mathbf{C_1}$–$\mathbf{C_3}$ in the range 252–300 nm with high molar extinction coefficient are associated with the localized π–π* transitions of the 2-(1H-benzimidazol-2-yl)quinoline and 2-phenylpyridine ligands. The band at around 365 nm is observed which is related to metal-to-ligand charge-transfer (MLCT) transition [40]. PL spectra of the compounds exhibit a broad emission band centered at 634 nm for $\mathbf{C_1}$, 645 nm for $\mathbf{C_2}$ and 636 nm for $\mathbf{C_3}$. The quantum yields of the compounds are found as 0.14 for $\mathbf{C_1}$, 0.11 for $\mathbf{C_2}$ and 0.10 for $\mathbf{C_3}$. The bathochromic shift of the emission of $\mathbf{C_2}$ relative to those $\mathbf{C_1}$ and $\mathbf{C_3}$ are attributed the electron donor properties of methyl groups [41].

The electrochemical measurements were performed using cyclic voltammetry in order to investigate the HOMO/LUMO energy levels and stability of iridium compounds. The compounds exhibit a reversible oxidation peak which is associated with the oxidation iridium metal (Fig. 2 and Table 2). The oxidation potential of $\mathbf{C_2}$ with methyl groups on 2-(1H-benzimidazol-2-yl)quinoline ligand of the compound is shifted to

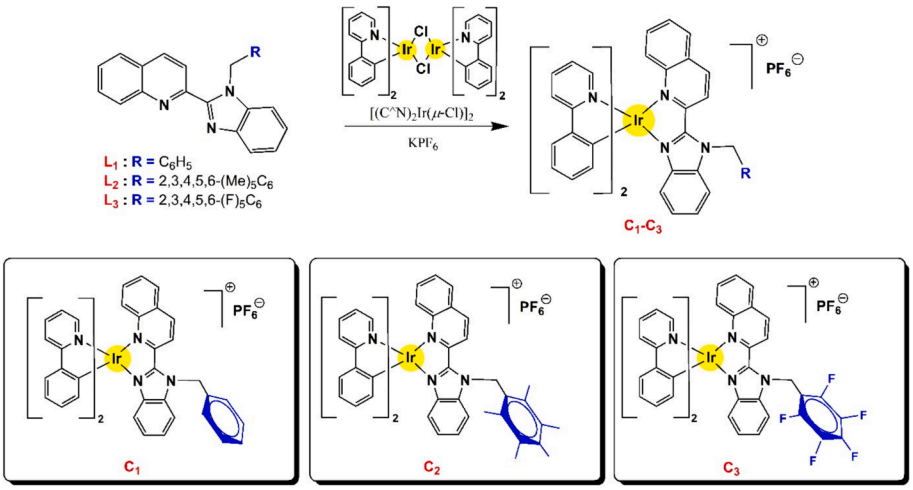

Scheme 1. Reaction scheme for the synthesis of the cyclometalated Ir(III) complexes bearing *N,N*-type 2-(2′-quinoly)benzimidazole ligands (C_1–C_3).

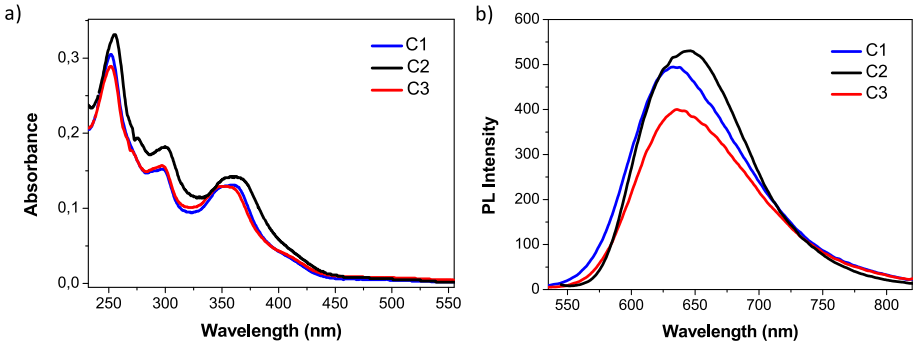

Fig. 1. (a) Absorption spectra and (b) PL spectra of 1 × 10^{-5} M solutions of C_1–C_3 in acetonitrile at room temperature. Excitation wavelengths are their lowest energy MLCT absorption maxima.

Table 2
Photophysical and electrochemical data of C_1–C_3 in acetonitrile.

Compound	$\lambda_{maks\ (Abs)}$ (nm) (ε/10^4 $M^{-1}.cm^{-1}$)	$\lambda_{maks\ (PL)}$ (nm)	E_{ox} (V)	HOMO (eV)	LUMO (eV)	Eg (eV)
C_1	252 (3.04); 298 (1.53); 360 (1.29)	634	1.34	−5.68	−2.97	2.71
C_2	255 (3.32); 300 (1.82); 365 (1.43)	645	1.24	−5.58	−2.89	2.69
C_3	252 (2.90); 298 (1.54); 359 (1.27)	636	1.32	−5.66	−2.98	2.68

cathodic area when compared to the C_1 and C_3 due to the electron donor properties of methyl groups. The HOMO and LUMO energy levels were determined by following equations [42,43]: E_{HOMO}=-e($E_{1/2(ox.,onset)}$ − $E_{1/2(Fe)}$ + 4.8) and E_{LUMO}=E_{HOMO}+Eg, including ferrocene value of 0.46 V *vs.* Ag/ Ag^+. The calculated HOMO and LUMO energy levels of the compounds are in the range of (−5.58)-(−5.68) eV and (−2.89-(−2.98)) eV, respectively. In consecutive voltammogram, the reversibility of oxidation peaks and no important change in peak potentials show the electrochemical stability of the compounds.

3.3. MTT assay

The cytotoxicity of C_1, C_2 and C_3 evaluated against two breast cancer cell line (MDA-MB-231 and MCF-7) and non-cancerous HEK293 cell line by the MTT assay. In the current study, different concentrations of the compounds (15.6–250 μM) were attended for cytotoxicity investigations. After 24 h of exposure, the cytotoxicity of C_1 to these cell lines (expressed as IC_{50} values) was found to be 11.76 μM for MDA-MB-231, 5.35 μM for MCF-7, and 17.73 μM for HEK293, respectively. The IC_{50} value of the C_3 was found to be 16.22 μM for MDA-MB-231, 8.85 μM for MCF-7, and 20.07 μM for HEK293 cells.

We observed that C_1 and C_3 exhibited a stronger cytotoxic effect on MDA-MB-231 and MCF-7 cells than the HEK293 cell line. It is worth noting that C_1 and C_3 showed a higher selectivity index (SI) for MCF-7 cells. Based on the ratio of the IC50 values for non-cancerous cells to breast cancer cells, C_3 was 1.23 times more cytotoxic to MDA-MB-231 cells and 2.26 times more cytotoxic to MCF-7 cells compared to HEK293 cells. Similarly, C_1 exhibited cytotoxicity that was 1.50 times higher against MDA-MB-231 cells and 3.31 times higher against MCF-7 cells than HEK293 cells (Table 3). Moreover, C_1 and C_3 exhibited an antiproliferative effect on MDA-MB-231 (IC_{50} = 11.76 and 16.22 μM, respectively) and MCF-7 (IC_{50} = 5.35 and 8.85 μM, respectively), which was better than cisplatin. C_2 did not affect the viability in comparison to C_1 and C_3 where we detected cytotoxic activity (Fig. 3). It is well established that side groups can affect the cytotoxicity of the compounds [44]. Therefore, the side groups of the studied iridium complexes are different, and their cytotoxic effects have been observed differently.

It is known and of interest that the activities of anticancer cyclometalated iridium(III) complexes is related to their ability to induce mitochondria-mediated cell death pathway, deregulation of cellular redox balance, and inhibition of protein interactions [45–47]. It can be said that these complexes, kinetically inert under physiological conditions, thereby exert their anticancer activity through non-covalent

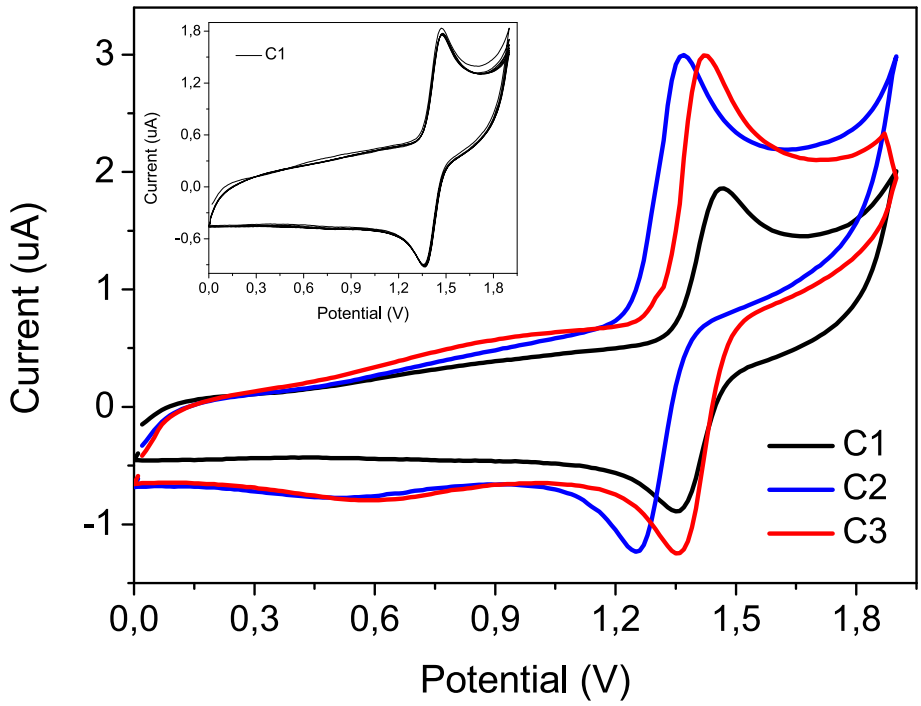

Fig. 2. Cyclic voltammograms of C_1–C_3 and consecutive cyclic voltammograms of C_1 (inset) in acetonitrile solution containing 0.1 M $TBAPF_6$ at a scan rate of 100 mVs^{-1}. Glassy carbon working electrode, silver wire reference electrode and Pt wire counter electrode were used in the three-electrode system.

Table 3
IC_{50} values and selectivity index of C_1, C_2, and C_3 on MDA-MB-231, MCF-7, and HEK293 cells.

	IC_{50} (μM) ± SD			Selectivity Index (SI)	
	MDA-MB-231	MCF-7	HEK293	HEK293/MDA-MB-231	HEK293/MCF-7
C_1	11.76 ± 0.56	5.35 ± 0.14	17.73 ± 0.09	1.50	3.31
C_2	>250	>250	>250	–	–
C_3	16.22 ± 0.08	8.85 ± 0.77	20.07 ± 0.28	1.23	2.26

interactions. In another study, iridium(III) complexes reduced cell proliferation in human gastric carcinoma SGC-7901 cells [48]. Similarly, half-sandwich iridium(III) complexes showed antiproliferative effects via disrupting mitochondrial membrane potential and inducing oxidative stress on MCF-7 breast cancer cells [49]. Moreover, different cyclometalated iridium(III) complexes showed anticancer activities on cancer cells that were similar to our results [49–53].

3.4. Colony formation

The colony formation assay was evaluated by seeding 1×10^3 cells and treating with IC_{50} dose of iridium(III) complexes for 24 h. Colonies were stained with 0.1 % crystal violet and counted by ImageJ software. Fig. 2 showed that C_1 and C_3 could inhibit the proliferation of breast cancer cells MDA-MB-231 and MCF-7 only after 24 h (Fig. 4).

In consistent with our results, iridium complexes was caused inhibition of cellular colonies of HeLa human cervical cancer cells [54]. Moreover, Liu et al. have showed that the cyclometalated iridium complex Ir-9-Ac inhibitory effects on colony formation on A549, A549R, A2780 and MCF-7 cells [55]. In another study, it was shown that cyclometalated iridium(III) complexes causes inhibition of the colony formation in A549 lung cancer cells [56].

3.5. Annexin V/PI staining

The APC Annexin V Apoptosis Detection Kit with 7-AAD was used to detect apoptosis. Cells showed a different pattern of cytotoxicity induced by C_1 and C_3 after 24 h of exposure. Although early-apoptotic and necrotic death were observed in MDA-MB-231 cells, late-apoptotic and necrotic death were seen in MCF-7 cells treated with iridium complexes (Fig. 5). As shown in Fig. 5a, the percentages of apoptotic cells were 10.2 % and 19 % in MDA-MB-231 cells for C_1 and C_3, respectively, compared with 11.1 % in the positive control ($P < 0.05$). Similarly, 26.5 % and 28.3 % in MCF-7 cells for C_1 and C_3, respectively, compared with 39 % in the positive control (Fig. 5b, $P < 0.05$). Moreover, treatment of iridium complexes led to an apparent increase in the number of necrotic cells.

In our experiments, we were able to show that the cytotoxic activity of cyclometalated iridium(III) complexes toward breast cancer cell can be attributed to the effective induction of different types of cell death including apoptosis (Fig. 5, Table 4).

3.6. Gene expression analysis

To determine the alteration of apoptosis pathways by the C_1 and C_3, a qRT-PCR array was used to evaluate the expression levels of the *Bax, Bcl-2, caspase 3, 8,* and *9* genes in MDA-MB-231 and MCF-7 cell lines. After the C_1 treatment, *Bax, caspase 3, 8,* and *9* mRNA levels were increased 1.59-, 1.65-, 2.5-, and 1.63- fold in MDA-MB-231 cells ($P < 0.05$), respectively. Similarly, *Bax, caspase 3, 8,* and *9* mRNA levels were increased 2.94-, 5.04-, 1.64-, and 1.43- fold in MDA-MB-231 cells, respectively. On the contrary, C_1 caused 57.0 and 31.2 % decreases in *Bcl-2* mRNA level in MDA-MB-231 and MCF-7 cell line when compared to the control group ($P < 0.05$), respectively. Besides, RT-PCR results showed C_3 treatment caused 1.32-, 1.87-, 3.82-, and 4.09- fold increases in *Bax, caspase 3, 8,* and *9* mRNA levels in the MDA-MB-231 cell line ($P < 0.05$), respectively. C_3 caused 1.15-, 1.46-, 1.55-, and 1.04- fold increases in *Bax, caspase 3, 8,* and *9* mRNA levels in MCF-7 cells, respectively. On the contrary, C_3 caused 53.5 and 30.2 % decreases in *Bcl-2* mRNA level in MDA-MB-231 and MCF-7 cell line ($P < 0.05$, Table 3),

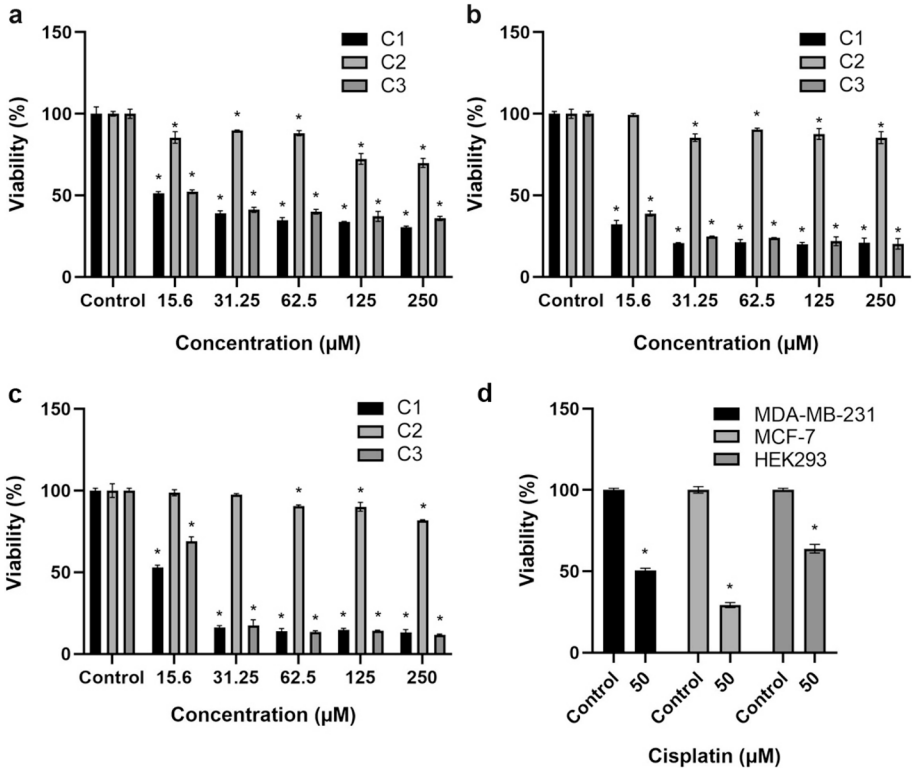

Fig. 3. The cytotoxic effects of C_1, C_2 and C_3 against **a.** MDA-MB-231, **b.** MCF-7, and **c.** HEK293 cells. **d.** Cisplatin (50 μM) was used as a positive control. Data were mean values of two independent replicates. *: $p < 0.05$ compared with the control group.

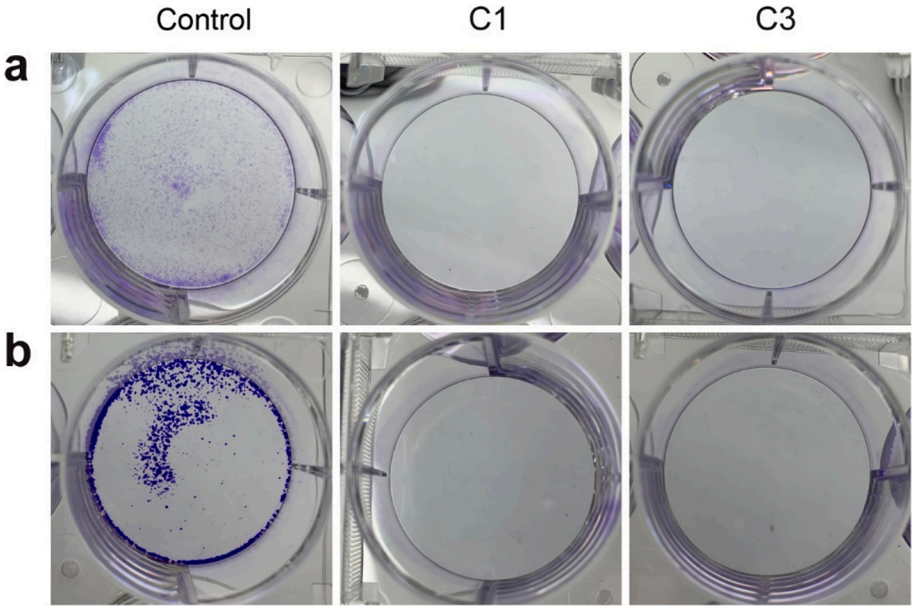

Fig. 4. Estimation of the proliferation of **a.** MDA-MB-231 and **b.** MCF-7 cells using the colony formation assay. The C_1 and C_3 compounds (IC_{50} concentrations) almost completely suppressed the colony formation.

respectively.

Apoptosis induction involves two pathways: the extrinsic pathway, dependent on death receptors, and the intrinsic pathway (mitochondria-dependent) [57,58]. The mitochondria-mediated intrinsic apoptotic pathway is primarily activated by the collapse of the mitochondrial membrane potential. Upon sense the cell death stimuli, mitochondria release cytochrome *c* into the cytosol, where it binds with *Apaf-1* and *caspase-9*, forming a complex termed the apoptosome [59]. This complex triggers the activation of downstream *caspases 3, -6,* and *-7*, as well as with other apoptotic effectors, consequently, the activation of the caspase-cascade system is the key event in mitochondria-dependent apoptosis [60].

We detected cyclometalated iridium(III) complexes that increased the pro-apoptotic mRNA levels and decreased anti-apoptotic mRNA levels. Fig. 6 showed that C_1 and C_3 compounds caused increases in the mRNA expression levels of *caspase 3, 8,* and *9* (pro-apoptotic) genes, and

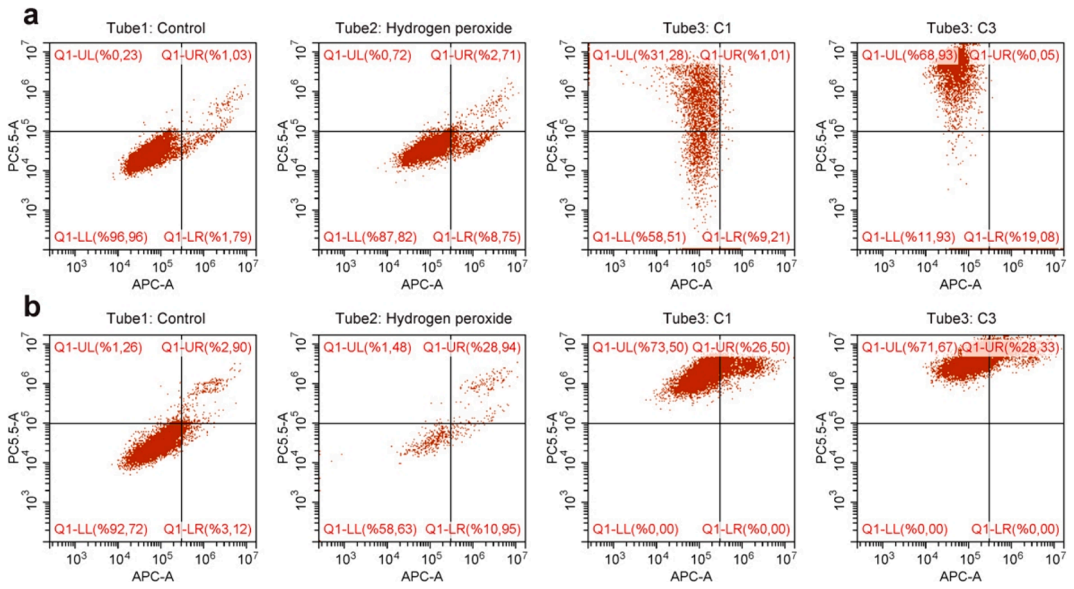

Fig. 5. a. MDA-MB-231 and **b.** MCF-7 cells were assessed by flow cytometry using the Annexin V-APC/7-AAD apoptosis assay after 24 h exposure. (Q1-UL: dead cells; Q1-UR: late apoptosis; Q1-LL: viable cells; Q1-LR: early apoptosis).

Table 4
Percentages of viable, apoptotic, and necrotic cells detected in MDA-MB-231 and MCF-7 cells after $\mathbf{C_1}$ and $\mathbf{C_3}$ treatment by flow cytometry analysis at 24 h.

Cell line	Group	Cell population (%)			
		Viable	Early apoptotic	Late apoptotic	Necrotic
MDA-MB-231	Control	96.96	1.79	1.03	0.23
	H_2O_2	87.82	8.75	2.71	0.72
	C_1	58.51	9.21	1.01	31.28
	C_3	11.93	19.08	0.05	68.93
MCF-7	Control	92.72	3.12	2.90	1.26
	H_2O_2	58.63	10.95	28.94	1.48
	C_1	0.00	0.00	26.50	73.50
	C_3	0.00	0.00	28.33	71.67

a decrease in *Bcl-2* (anti-apoptotic) gene expression. $\mathbf{C_3}$ at a concentration of 8.85 μM increased the expression of *caspase 9* (409.8 %) in MCF-7 cells more so than $\mathbf{C_1}$ (Fig. 6). Moreover, treatment of iridium(III) complexes caused an increase in *Bax/Bcl-2* ratio as well in both cell lines. All these findings indicated that the cell death caused by these compounds involved both intrinsic and extrinsic pathways of apoptosis. In accordance with our results, simultaneous occurrences of both forms of cell death are observed upon exposure to certain stimuli [61].

Furthermore, several previous studies proposed that necrotic cell death execution occurs independently of caspase activity [62–64]. However, in the breast cancer cell model treated with iridium complexes in this study, caspase activation induced concurrently with necrosis. These findings suggest that apoptosis and necrosis may share common characteristics, including caspase activation and *Bcl-2* family proteins. The result of this study demonstrated that iridium complexes exert cytotoxic effects by inducing necrosis and apoptosis in the MDA-MB-231 and MCF-7 cells through a mitochondria-associated pathway.

4. Conclusion

In this work, we have described the synthesis, characterization, cytotoxicity, and apoptosis of iridium compounds bearing 2-(1H-benzimidazol-2-yl)quinoline ligands. The compounds were synthesized using a bridge-splitting reaction of $Ir_2(ppy)_4Cl_2$ dimer with the corresponding 2-(1H-benzimidazol-2-yl)quinoline ligand in 2-ethoxyethanol. Our studies showed that $\mathbf{C_1}$ and $\mathbf{C_3}$ exhibited greater cytotoxic and apoptotic activity in MDA-MB-231 and MCF-7 cell lines. On the other hand, the different patterns observed in the flow cytometry analysis provided significant insights into the cell death induced by the complexes. The results in this study indicate that cyclometalated iridium compounds may have significant potential for anticancer activity. But, they should be needed further experiments to test this hypothesis.

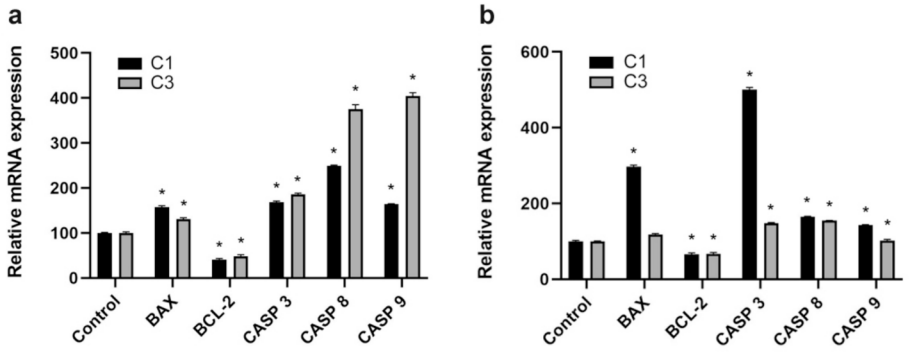

Fig. 6. *Bax*, *Bcl-2*, *caspase 3*, *8*, and *9* mRNA levels in MDA-MB-231 and MCF-7 cells. Individual gene expression levels were normalized by using GAPDH. Values indicated with stars are statistically significant different from control group (*$p < 0.05$).

CRediT authorship contribution statement

Cigdem Sahin: Writing – review & editing, Writing – original draft. **Dogukan Mutlu:** Writing – review & editing, Writing – original draft. **Ahmet Erdem:** Writing – original draft. **Rafet Kilincarslan:** Writing – review & editing, Writing – original draft. **Sevki Arslan:** Writing – original draft.

Declaration of competing interest

The authors declare the following financial interests/personal relationships which may be considered as potential competing interests: Cigdem Sahin reports financial support was provided by Istanbul Medeniyet University. Sevki Arslan reports financial support was provided by Istanbul Medeniyet University. Rafet Kilincarslan reports financial support was provided by Pamukkale University. If there are other authors, they declare that they have no known competing financial interests or personal relationships that could have appeared to influence the work reported in this paper.

Acknowledgements

The synthesis and anticancer studies of the iridium complexes bearing 2-(1H-benzimidazol-2-yl)quinoline have been supported by the Research Fund of Istanbul Medeniyet University (Project Number: F-GAP-2022-1813). The synthesis of 2-(1H-benzimidazol-2-yl)quinoline ligands part of this paper has been supported by Pamukkale University Scientific Research Projects Commission (Project No: 2014FEBE035, 2016FEBE013 and 2017FEBE042).

Appendix A. Supplementary material

Supplementary data to this article can be found online at https://doi.org/10.1016/j.bioorg.2024.107706.

References

[1] F. Bray, M. Laversanne, H. Sung, J. Ferlay, R.L. Siegel, I. Soerjomataram, A. Jemal, Global cancer statistics 2022: GLOBOCAN estimates of incidence and mortality worldwide for 36 cancers in 185 countries, CA Cancer J. Clin. 74 (2024) (2022) 229–263, https://doi.org/10.3322/caac.21834.
[2] R.L. Siegel, K.D. Miller, N.S. Wagle, A. Jemal, Cancer statistics, 2023, CA. Cancer J. Clin. 73 (2023) 17–48, https://doi.org/10.3322/caac.21763.
[3] F. Martínez-Jiménez, F. Muiños, I. Sentís, J. Deu-Pons, I. Reyes-Salazar, C. Arnedo-Pac, L. Mularoni, O. Pich, J. Bonet, H. Kranas, A. Gonzalez-Perez, N. Lopez-Bigas, A compendium of mutational cancer driver genes, Nat. Rev. Cancer 20 (2020) 555–572, https://doi.org/10.1038/s41568-020-0290-x.
[4] D.T. Debela, S.G. Muzazu, K.D. Heraro, M.T. Ndalama, B.W. Mesele, D.C. Haile, S. K. Kitui, T. Manyazewal, New approaches and procedures for cancer treatment: current perspectives, 205031212110343, SAGE Open Med. 9 (2021), https://doi.org/10.1177/20503121211034366.
[5] U. Anand, A. Dey, A.K.S. Chandel, R. Sanyal, A. Mishra, D.K. Pandey, V. De Falco, A. Upadhyay, R. Kandimalla, A. Chaudhary, J.K. Dhanjal, S. Dewanjee, J. Vallamkondu, J.M. Pérez De La Lastra, Cancer chemotherapy and beyond: current status, drug candidates, associated risks and progress in targeted therapeutics, Genes Dis. 10 (2023) 1367–1401, https://doi.org/10.1016/j.gendis.2022.02.007.
[6] E.A. Moharram, S.M. El-Sayed, H.A. Ghabbour, H.I. El-Subbagh, Synthesis, molecular modeling simulations and anticancer activity of some new Imidazo[2,1-b]thiazole analogues as EGFR/HER2 and DHFR inhibitors, Bioorg. Chem. 150 (2024) 107538, https://doi.org/10.1016/j.bioorg.2024.107538.
[7] W. Liu, R. Gust, Update on metal N-heterocyclic carbene complexes as potential anti-tumor metallodrugs, Coord. Chem. Rev. 329 (2016) 191–213, https://doi.org/10.1016/j.ccr.2016.09.004.
[8] S. Ghosh, Cisplatin: the first metal based anticancer drug, Bioorg. Chem. 88 (2019) 102925, https://doi.org/10.1016/j.bioorg.2019.102925.
[9] A. Zoń, I. Bednarek, Cisplatin in ovarian cancer treatment—known limitations in therapy force new solutions, Int. J. Mol. Sci. 24 (2023) 7585, https://doi.org/10.3390/ijms24087585.
[10] X. Yao, K. Panichpisal, N. Kurtzman, K. Nugent, Cisplatin nephrotoxicity: a review, Am. J. Med. Sci. 334 (2007) 115–124, https://doi.org/10.1097/MAJ.0b013e31812dfe1e.
[11] J. Zhou, Y. Kang, L. Chen, H. Wang, J. Liu, S. Zeng, L. Yu, The drug-resistance mechanisms of five platinum-based antitumor agents, Front. Pharmacol. 11 (2020) 343, https://doi.org/10.3389/fphar.2020.00343.
[12] G. Fang, A. Zhang, L. Zhu, Q. Wang, F. Sun, B. Tang, Nanocarriers containing platinum compounds for combination chemotherapy, Front. Pharmacol. 13 (2022) 1050928, https://doi.org/10.3389/fphar.2022.1050928.
[13] Y. Li, B. Liu, C.-X. Xu, L. He, Y.-C. Wan, L.-N. Ji, Z.-W. Mao, Mitochondria-targeted phosphorescent cyclometalated iridium(III) complexes: synthesis, characterization, and anticancer properties, J. Biol. Inorg. Chem. 25 (2020) 597–607, https://doi.org/10.1007/s00775-020-01783-2.
[14] J.-J. Cao, Y. Zheng, X.-W. Wu, C.-P. Tan, M.-H. Chen, N. Wu, L.-N. Ji, Z.-W. Mao, Anticancer cyclometalated iridium(III) complexes with planar ligands: mitochondrial DNA damage and metabolism disturbance, J. Med. Chem. 62 (2019) 3311–3322, https://doi.org/10.1021/acs.jmedchem.8b01704.
[15] L. He, K.-N. Wang, Y. Zheng, J.-J. Cao, M.-F. Zhang, C.-P. Tan, L.-N. Ji, Z.-W. Mao, Cyclometalated iridium(iii) complexes induce mitochondria-derived paraptotic cell death and inhibit tumor growth in vivo, Dalton Trans. 47 (2018) 6942–6953, https://doi.org/10.1039/C8DT00783G.
[16] Q. Zhao, C. Huang, F. Li, Phosphorescent heavy-metal complexes for bioimaging, Chem. Soc. Rev. 40 (2011) 2508, https://doi.org/10.1039/c0cs00114g.
[17] L. Huang, P.-K.-K. Leung, L.-C.-C. Lee, G.-X. Xu, Y.-W. Lam, K.-K.-W. Lo, Photofunctional cyclometallated iridium(iii) polypyridine methylsulfone complexes as sulfhydryl-specific reagents for bioconjugation, bioimaging and photocytotoxic applications, Chem. Commun. 58 (2022) 10162–10165, https://doi.org/10.1039/D2CC02405E.
[18] Y. Li, K.-N. Wang, L. He, L.-N. Ji, Z.-W. Mao, Synthesis, photophysical and anticancer properties of mitochondria-targeted phosphorescent cyclometalated iridium(III) N-heterocyclic carbene complexes, J. Inorg. Biochem. 205 (2020) 110976, https://doi.org/10.1016/j.jinorgbio.2019.110976.
[19] J.S. Nam, M.-G. Kang, J. Kang, S.-Y. Park, S.J.C. Lee, H.-T. Kim, J.K. Seo, O.-H. Kwon, M.H. Lim, H.-W. Rhee, T.-H. Kwon, Endoplasmic reticulum-localized iridium(III) complexes as efficient photodynamic therapy agents via protein modifications, J. Am. Chem. Soc. 138 (2016) 10968–10977, https://doi.org/10.1021/jacs.6b05302.
[20] Y. Yang, C.-M. Wang, F.-H. Pan, Q.-P. Qin, Q.-J. Xie, Q. Chen, H. Liang, Synthesis and biological evaluation of mixed-ligand cyclometalated iridium(iii)–quinoline complexes, Dalton Trans. 50 (2021) 16273–16280, https://doi.org/10.1039/D1DT02416G.
[21] X. Liu, Y. Han, X. Ge, Z. Liu, Imidazole and benzimidazole modified half-sandwich iridium^{III} N-heterocyclic carbene complexes: synthesis, anticancer application, and organelle targeting, Front. Chem. 8 (2020) 182, https://doi.org/10.3389/fchem.2020.00182.
[22] Y.T. Lee, Y.J. Tan, C.E. Oon, Benzimidazole and its derivatives as cancer therapeutics: the potential role from traditional to precision medicine, Acta Pharm. Sin. B 13 (2023) 478–497, https://doi.org/10.1016/j.apsb.2022.09.010.
[23] A. Abdullah Al Awadh, Biomedical applications of selective metal complexes of indole, benzimidazole, benzothiazole and benzoxazole: a review (From 2015 to 2022), Saudi Pharm. J. 31 (2023) (2015) 101698, https://doi.org/10.1016/j.jsps.2023.101698.
[24] T.-R. Chen, Synthesis, structure, and field-effect property of 2-(benzimidazol-2-yl) quinoline, Mater. Lett. 59 (2005) 1050–1052, https://doi.org/10.1016/j.matlet.2004.12.002.
[25] M.A. Bennett, T.-N. Huang, T.W. Matheson, A.K. Smith, S. Ittel, W. Nickerson, 16. (η^6-Hexamethylbenzene)Ruthenium Complexes, in: J.P. Fackler (Ed.), Inorg. Synth., 1st ed., Wiley, 1982, pp. 74–78, doi: 10.1002/9780470132524.ch16.
[26] A. Erdem, R. Kılınçarslan, Ç. Şahin, O. Dayan, N. Özdemir, Synthesis, thermal, electrochemical and catalytic behavior toward transfer hydrogenation investigations of the half-sandwich RuII complexes with 2-(2′-quinolyl) benzimidazoles, J. Mol. Struct. 1220 (2020) 128556, https://doi.org/10.1016/j.molstruc.2020.128556.
[27] O. Dayan, M. Tercan, N. Özdemir, Syntheses and molecular structures of novel Ru (II) complexes with bidentate benzimidazole based ligands and their catalytic efficiency for oxidation of benzyl alcohol, J. Mol. Struct. 1123 (2016) 35–43, https://doi.org/10.1016/j.molstruc.2016.06.017.
[28] S. Sprouse, K.A. King, P.J. Spellane, R.J. Watts, Photophysical effects of metal-carbon.sigma. bonds in ortho-metalated complexes of iridium(III) and rhodium (III), J. Am. Chem. Soc. 106 (1984) 6647–6653, https://doi.org/10.1021/ja00334a031.
[29] T.E. Knight, A.P. Goldstein, M.K. Brennaman, T. Cardolaccia, A. Pandya, J. M. DeSimone, T.J. Meyer, Influence of the fluid-to-film transition on photophysical properties of MLCT excited states in a polymerizable dimethacrylate fluid, J. Phys. Chem. B 115 (2011) 64–70, https://doi.org/10.1021/jp107077t.
[30] L. He, J. Qiao, L. Duan, G. Dong, D. Zhang, L. Wang, Y. Qiu, Toward highly efficient solid-state white light-emitting electrochemical cells: blue-green to red emitting cationic iridium complexes with imidazole-type ancillary ligands, Adv. Funct. Mater. 19 (2009) 2950–2960, https://doi.org/10.1002/adfm.200900723.
[31] C. Sahin, D. Mutlu, F. Nasirli, G. Mahmoudi, F.I. Zubkov, S. Arslan, N.M. Dogan, New iridium bis-terpyridine complexes: synthesis, characterization, antibiofilm and anticancer potentials, Biometals 34 (2021) 701–713, https://doi.org/10.1007/s10534-021-00307-y.
[32] D. Mutlu, M. Seçme, Ş. Arslan, Effects of usnic acid on cytotoxicity, colony formation and migration in SK-UT-1 human uterine leiomyosarcoma cells, Süleyman Demirel Üniversitesi Fen Edeb Fakültesi Fen Derg 18 (2023) 195–202, https://doi.org/10.29233/sdufeffd.1250542.
[33] M. Secme, D. Mutlu, L. Elmas, S. Arslan, Assessing effects of caffeic acid on cytotoxicity, apoptosis, invasion, GST enzyme activity, oxidant, antioxidant status and micro-RNA expressions in HCT116 colorectal cancer cells, South Afr. J. Bot. 157 (2023) 19–26, https://doi.org/10.1016/j.sajb.2023.03.046.

[34] R. Liman, A.N. Kursunlu, M. Ozmen, S. Arslan, D. Mutlu, E.S. Istifli, Y. Acikbas, Synthesis of water soluble symmetric and asymmetric pillar[5]arene derivatives: cytotoxicity, apoptosis and molecular docking studies, J. Mol. Struct. 1265 (2022) 133482, https://doi.org/10.1016/j.molstruc.2022.133482.
[35] P. Garg, U. De, N. Dehury, H.S. Kim, S. Patra, Cyclometallated imidazo-phenanthroline iridium complexes and their anticancer activity, J. Chem. Sci. 130 (2018) 76, https://doi.org/10.1007/s12039-018-1492-6.
[36] C. Liu, L. Yu, Y. Liu, F. Li, M. Zhou, NMR study on iridium(III) complexes for identifying disulfonate substituted bathophenanthroline regio-isomers, Magn. Reson. Chem. 49 (2011) 816–823, https://doi.org/10.1002/mrc.2815.
[37] M. Martínez-Alonso, J. Cerdá, C. Momblona, A. Pertegás, J.M. Junquera-Hernández, A. Heras, A.M. Rodríguez, G. Espino, H. Bolink, E. Ortí, Highly stable and efficient light-emitting electrochemical cells based on cationic iridium complexes bearing arylazole ancillary ligands, Inorg. Chem. 56 (2017) 10298–10310, https://doi.org/10.1021/acs.inorgchem.7b01167.
[38] C. Sahin, M. Sahin, New iridium complexes(III) bearing 2-phenylimidazo[4,5-f][1,10]-phenanthroline ligand: synthesis, characterization, electrochemical and photoluminescence studies, J. Mol. Struct. 1226 (2021) 129415, https://doi.org/10.1016/j.molstruc.2020.129415.
[39] F.O. Garces, R.J. Watts, ^{1}H and ^{13}C NMR assignments with coordination-induced shift calculations of carbon σ-bonded *ortho* -metalated rhodium(III) and iridium (III) complexes, Magn. Reson. Chem. 31 (1993) 529–536, https://doi.org/10.1002/mrc.1260310603.
[40] R. Cao, J. Jia, X. Ma, M. Zhou, H. Fei, Membrane localized iridium(III) complex induces endoplasmic reticulum stress and mitochondria-mediated apoptosis in human cancer cells, J. Med. Chem. 56 (2013) 3636–3644, https://doi.org/10.1021/jm4001665.
[41] K. Hasan, A.K. Bansal, I.D.W. Samuel, C. Roldán-Carmona, H.J. Bolink, E. Zysman-Colman, Tuning the emission of cationic iridium (III) complexes towards the red through methoxy substitution of the cyclometalating ligand, Sci. Rep. 5 (2015) 12325, https://doi.org/10.1038/srep12325.
[42] A. Shafiee, M. Salleh, M. Yahaya, Determination of HOMO and LUMO of [6,6]-phenyl C61-butyric acid 3-ethylthiophene ester and poly (3-octyl-thiophene-2, 5-diyl) through voltametry characterization, accessed June 25, 2024, Sains Malays. 40 (2011) 173–176, https://www.semanticscholar.org/paper/Determination-of-HOMO-and-LUMO-of-%5B6%2C6%5D-phenyl-acid-Shafiee-Salleh/c50f0853229859a064f6393f37ef05ad3f7dad56.
[43] M. Lin, D. Li, X. Wang, C. Luo, Q. Ling, Synthesis and optical properties of white phosphorescent carbazole - iridium copolymers, J. Macromol. Sci. Part A 53 (2016) 222–226, https://doi.org/10.1080/10601325.2016.1143317.
[44] S.K. Liew, S. Malagobadan, N.M. Arshad, N.H. Nagoor, A review of the structure-activity relationship of natural and synthetic antimetastatic compounds, Biomolecules 10 (2020) 138, https://doi.org/10.3390/biom10010138.
[45] J. Zhao, S. Sun, X. Li, W. Zhang, S. Gou, Enhancing photodynamic therapy efficacy of upconversion-based nanoparticles conjugated with a long-lived triplet excited state iridium(III)-naphthalimide complex: toward highly enhanced hypoxia-inducible factor-1, ACS Appl. Bio Mater. 3 (2020) 252–262, https://doi.org/10.1021/acsabm.9b00774.
[46] L. Wang, R. Guan, L. Xie, X. Liao, K. Xiong, T.W. Rees, Y. Chen, L. Ji, H. Chao, An ER-targeting iridium(III) complex that induces immunogenic cell death in non-small-cell lung cancer, Angew. Chem. Int. Ed. 60 (2021) 4657–4665, https://doi.org/10.1002/anie.202013987.
[47] Y. Wu, J. Liu, M. Shao, P. Zhang, S. Song, G. Yang, X. Liu, Z. Liu, Cyclometalated iridium(III) dithioformic acid complexes as mitochondria-targeted imaging and anticancer agents, J. Inorg. Biochem. 233 (2022) 111855, https://doi.org/10.1016/j.jinorgbio.2022.111855.
[48] L. Tian, Y. Zhang, H. Zhang, Y. Zhou, W. Li, Y. Yuan, J. Hao, L. Yang, Y. Liu, Synthesis and evaluation of iridium(III) complexes on antineoplastic activity against human gastric carcinoma SGC-7901 cells, J. Biol. Inorg. Chem. 26 (2021) 705–714, https://doi.org/10.1007/s00775-021-01895-3.
[49] A.C. Carrasco, V. Rodríguez-Fanjul, A. Habtemariam, A.M. Pizarro, Structurally strained half-sandwich iridium(III) complexes as highly potent anticancer agents, J. Med. Chem. 63 (2020) 4005–4021, https://doi.org/10.1021/acs.jmedchem.9b02000.
[50] B.-B. Chen, N.-L. Pan, J.-X. Liao, M.-Y. Huang, D.-C. Jiang, J.-J. Wang, H.-J. Qiu, J.-X. Chen, L. Li, J. Sun, Cyclometalated iridium(III) complexes as mitochondria-targeted anticancer and antibacterial agents to induce both autophagy and apoptosis, J. Inorg. Biochem. 219 (2021) 111450, https://doi.org/10.1016/j.jinorgbio.2021.111450.
[51] J.-J. Lu, X.-R. Ma, K. Xie, M.-R. Chen, B. Huang, R.-T. Li, R.-R. Ye, Lysosome-targeted cyclometalated iridium(III) complexes: JMJD inhibition, dual induction of apoptosis, and autophagy, Metallomics 14 (2022) mfac068, https://doi.org/10.1093/mtomcs/mfac068.
[52] Y. Yang, C.-M. Wang, H.-S. Cao, Z. Zhou, Q.-J. Xie, Q.-P. Qin, Q. Chen, Novel 4-/5-bromo-8-hydroxyquinoline cyclometalated iridium(III) complexes as highly potent anticancer and bioimaging agents, Inorg. Chem. Commun. 142 (2022) 109609, https://doi.org/10.1016/j.inoche.2022.109609.
[53] B. Liu, Z. Chen, Y. Li, X.-F. Du, W. Zhang, W. Zhang, Y. Lai, Y. Li, Brominated cyclometalated iridium(iii) complexes for mitochondrial immobilization as potential anticancer agents, Dalton Trans. 51 (2022) 7650–7657, https://doi.org/10.1039/D2DT00587E.
[54] F.-X. Wang, M.-H. Chen, Y.-N. Lin, H. Zhang, C.-P. Tan, L.-N. Ji, Z.-W. Mao, Dual functions of cyclometalated iridium(III) complexes: anti-metastasis and lysosome-damaged photodynamic therapy, ACS Appl. Mater. Interfaces 9 (2017) 42471–42481, https://doi.org/10.1021/acsami.7b10258.
[55] L. Liu, J. Chen, M.-M. Wang, Y. Huang, Y. Qian, X. Xue, Z. Su, H.-K. Liu, The cyclometalated iridium (III) complex based on 9-Anthracenecarboxylic acid as a lysosomal-targeted anticancer agent, J. Inorg. Biochem. 235 (2022) 111913, https://doi.org/10.1016/j.jinorgbio.2022.111913.
[56] Y. Gu, H. Wen, L. Bai, Y. Zhou, H. Zhang, L. Tian, Y. Zhang, J. Hao, Y. Liu, Exploring anticancer efficiency of mitochondria-targeted cyclometalated iridium (III) complexes, J. Inorg. Biochem. 212 (2020) 111215, https://doi.org/10.1016/j.jinorgbio.2020.111215.
[57] E. Beurel, R.S. Jope, The paradoxical pro- and anti-apoptotic actions of GSK3 in the intrinsic and extrinsic apoptosis signaling pathways, Prog. Neurobiol. 79 (2006) 173–189, https://doi.org/10.1016/j.pneurobio.2006.07.006.
[58] F. Wachter, M. Grunert, C. Blaj, D.M. Weinstock, I. Jeremias, H. Ehrhardt, Impact of the p53 status of tumor cells on extrinsic and intrinsic apoptosis signaling, Cell Commun. Signal 11 (2013) 27, https://doi.org/10.1186/1478-811X-11-27.
[59] X. Luo, I. Budihardjo, H. Zou, C. Slaughter, X. Wang, Bid, a Bcl2 interacting protein, mediates cytochrome c release from mitochondria in response to activation of cell surface death receptors, Cell 94 (1998) 481–490, https://doi.org/10.1016/S0092-8674(00)81589-5.
[60] C. Adrain, S.J. Martin, The mitochondrial apoptosome: a killer unleashed by the cytochrome seas, Trends Biochem. Sci. 26 (2001) 390–397, https://doi.org/10.1016/S0968-0004(01)01844-8.
[61] H. Shibuya, Y. Kato, M. Saito, T. Isobe, R. Tsuboi, M. Koga, H. Toyota, J. Mizuguchi, Induction of apoptosis and/or necrosis following exposure to antitumour agents in a melanoma cell line, probably through modulation of Bcl-2 family proteins, Melanoma Res. 13 (2003) 457–464, https://doi.org/10.1097/00008390-200310000-00004.
[62] C. Artus, H. Boujrad, A. Bouharrour, M.-N. Brunelle, S. Hoos, V.J. Yuste, P. Lenormand, J.-C. Rousselle, A. Namane, P. England, H.K. Lorenzo, S.A. Susin, AIF promotes chromatinolysis and caspase-independent programmed necrosis by interacting with histone H2AX, EMBO J. 29 (2010) 1585–1599, https://doi.org/10.1038/emboj.2010.43.
[63] L. Cabon, P. Galán-Malo, A. Bouharrour, L. Delavallée, M.-N. Brunelle-Navas, H. K. Lorenzo, A. Gross, S.A. Susin, BID regulates AIF-mediated caspase-independent necroptosis by promoting BAX activation, Cell Death Differ. 19 (2012) 245–256, https://doi.org/10.1038/cdd.2011.91.
[64] J. Lou, Y. Zhou, Z. Feng, M. Ma, Y. Yao, Y. Wang, Y. Deng, Y. Wu, Caspase-independent regulated necrosis pathways as potential targets in cancer management, Front. Oncol. 10 (2021) 616952, https://doi.org/10.3389/fonc.2020.616952.